AIAA JOURNAL
Vol. 44, No. 6, June 2006

Numerical Simulations of Fan Interaction Noise Using a Hybrid Approach

C. Polacsek,* S. Burguburu,† S. Redonnet,‡ and M. Terracol‡
ONERA, 92322 Châtillon, France

A source-to-far-field computation procedure aimed at predicting the noise generated by rotor–stator fan interactions is presented here. Interaction noise sources are assessed using a three-dimensional Reynolds-averaged Navier–Stokes (RANS) code. A modal expansion is applied to the computational fluid dynamics (CFD) data, and a source model is used to link the CFD to an Euler code simulating the acoustic propagation. Far-field noise is classically obtained by means of a Kirchhoff integral. The source model is detailed and validated over a selected benchmark. Then the hybrid method is applied to a turbofan model, tested in the German–Dutch Wind Tunnel. Simulations are compared to boundary element method computations previously performed and used here to validate the no-flow solution. Interacting cut-on mode amplitude deduced from CFD output postprocessing is adjusted to fit in-duct measurements on the outer wall. The predicted radiation field is related to the directivity patterns measured at several axial positions upstream of the fan inlet and fairly good agreement is found using the RANS/Euler/Kirchhoff procedure.

Nomenclature

$A_{m\mu}$	=	normalized amplitude of expanded Green's function with respect to a mode (m, μ)
$C_{m\mu}$	=	Hankel-like eigenfunction of order m, $(aJ_m + bY_m)$
c_0	=	sound speed
d	=	source-observer distance in the translating propagation medium, $\sqrt{[(x_1 - y_1)^2 + \beta^2(x_2 - y_2)^2 + \beta^2(x_3 - y_3)^2]}$
G	=	Green's function (expressed in the time domain)
$G_{m\mu}$	=	Green's function expanded over mode (m, μ)
G_ω	=	harmonic Green's function (frequency domain)
h	=	hub-to-tip ratio
K	=	total wave number
k	=	axial wave number
M	=	uniform mean flow Mach number (along z axis)
m	=	spinning mode order, that is, circumferential mode
n_i	=	coordinates of outside normal to the Kirchhoff surface
$p_{m\mu}$	=	Fourier–Bessel transformed pressure with respect to mode (m, μ)
p_ω	=	harmonic pressure
q	=	monopole (harmonic point-source) amplitude
(r, θ, z)	=	cylindrical coordinates in the duct frame
(r_s, θ_s, z_s)	=	source coordinates in the duct; θ_s and z_s are set equal to zero in the equations
S_k	=	Kirchhoff surface
t	=	observer time
U_0	=	uniform mean flow velocity (along z axis)
x_i	=	observer x coordinates in the wind-tunnel frame
y_i	=	source y coordinates in the wind-tunnel frame
$\alpha_{m\mu}$	=	eigenvalues for the mode (m, μ) solution of a Bessel equation
β	=	Lorentz factor, $\sqrt{(1 - M^2)}$
μ	=	radial mode order
(ρ, u, p)	=	density, velocity, and pressure disturbances (acoustic pressure in the linear domain)
(ρ_0, p_0)	=	mean density and mean pressure
σ	=	Lorentz-modified distance between source and observer, $[d - M(x_1 - y_1)]/\beta^2$
τ	=	emission time
φ	=	angle between source–observer direction and normal to S_k
ω	=	angular pulsation

Received 6 May 2004; revision received 31 May 2005; accepted for publication 29 November 2005.

*Research Engineer, Numerical Simulations and Aeroacoustics Department; cyril.polacsek@onera.fr.

†Research Engineer, Applied Aerodynamics Department; stephane.burguburu@onera.fr.

‡Research Engineer, Numerical Simulations and Aeroacoustics Department.

I. Introduction

DISCRETE-FREQUENCY tones generated by unsteady blade row interactions are of particular concern in the design of advanced turbine engines. For subsonic fans, the acoustic tones are usually 10–15 dB above the broadband level and are mainly due to wake interaction between rotor and stator. For this reason, a source-to-far-field computation chain has been proposed by ONERA for predicting the noise generated by rotor–stator interactions and radiated from the engine inlet or from the exhaust (Fig. 1).

Noise sources and near-field perturbations in the vicinity of the fan are assessed using a three-dimensional Reynolds-averaged Navier–Stokes (RANS) solver from the ONERA platform ELSA[1–3] developed for turbomachinery applications. As is commonly adopted by many authors from the aeroacoustics community,[4–13] a modal approach based on the expansion of computational fluid dynamics (CFD) perturbations over incoming and outgoing Fourier–Bessel harmonics is used to match the CFD and computational aeroacoustics (CAA) domains, assuming a uniform mean flow and an annular geometry in the matching region. The main originality here is that the outgoing modes are regenerated in terms of equivalent monopoles, to be entered as source inputs in the CAA, rather than directly use the pressure mode profile as a boundary condition. This point is underlined in the paper. The CAA is performed by using the ONERA multipurpose platform SABRINA,[14–16] whose specificity for acoustics is to solve disturbances Euler equations (DEE) with a sixth-order scheme in space. When isentropic subsonic inlet flows are considered, solutions should be roughly equivalent to those computed using standard linearized Euler equations (LEE). DEE calculation is classically coupled to a Kirchhoff integral (see Ref. 17), written in the frequency domain, to extrapolate the solution up to the far field. These simulations are also compared to successful results[18,19] previously obtained by coupling the CFD to a boundary element method (BEM) commercial code, neglecting mean flow velocity.

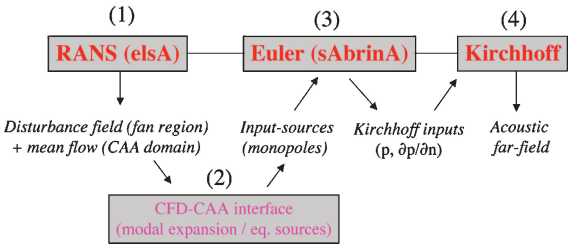

Fig. 1 Source-to-far-field computation procedure.

First, in Sec. II the CFD and CAA codes and the Kirchhoff routine are described. In particular, main specificities required for a reliable simulation of both the noise source generation and the acoustic propagation are emphasized. Second, in Sec. III the postprocessing of RANS solution is described, aiming at providing the source inputs for Euler computations. The method is validated in Sec. IV by comparing analytical and numerical solutions relative to a benchmark proposed in Ref. 18 (validated for a fluid at rest using BEM) and including convection effects using DEE. The computation procedure is finally applied in Sec. V to a fan model tested in the DNW–LLF anechoic wind tunnel.[20] The fan model consists in a one-stage simplified compressor (rods instead of blades) of annular geometry. Modal analyses and far-field directivity patterns are available, and both are used to validate the computations. The modal spectrum deduced from the simulations is compared to the measured spectrum, deduced from modal analysis performed during the tests, to adjust the in-duct pressure amplitude on the outer wall. The methodology employed for the RANS/Euler coupling, that is, source-term injection instead of the usual boundary condition approach, is expected to take into account significant reflections on the turbofan inlet and outlet, giving rise to standing waves inside the duct, as detected during the tests. The acoustic radiation computed in the upstream direction is compared to the noise measurements by plotting the directivity patterns at the blade passing frequency (BPF) at several positions of the microphone rake. Upstream radiation on BPF then is compared to the measured directivity patterns. Hence, reliability of the present simulations is discussed.

II. Numerical Tools

A. RANS Computations

CFD calculation is performed using the three-dimensional Navier–Stokes solver from ELSA that solves the compressible RANS equations in the relative frame. Space discretization is ensured using Jameson's second-order-centered scheme with a cell-vertex approach. Time integration is based on a four-step Runge–Kutta scheme. Boundary conditions are based on the conventional characteristic relations. Unsteady computations (rotor–stator interaction problem) are performed using a phase-lagged approach,[21] which permits the computation of the stage aerodynamics over a single rotor and stator passage.

To reduce the computational effort without altering the accuracy of noise sources and outgoing perturbations in the vicinity of the rows, the CFD domain can be limited to the fan region. (Inlet and outlet geometry do not necessarily have to be meshed.) This is relevant to the CFD/CAA proposed coupling, which only requires outgoing disturbances. This point may be very interesting for two linked reasons:

1) Current CFD solvers are unable to provide accurately a total disturbance field including incoming waves due to the physical reflections on the inlet or outlet.

2) The CFD disturbance field solution often is contaminated by incoming waves due to nonphysical, that is, numerical, reflections on the grid boundaries, which can be removed by using a wave-splitting technique as is done in this study (Sec. V).

A special care has to be paid to the mesh density between the rotor and stator to capture the rotor wake and its interaction with the outlet guide vanes. Grid density is reduced in the region upstream of the rotor, with a minimum resolution of 40 points per acoustic wavelength (according to the parametric studies achieved in TurboNoiseCFD) and is stretched up to the mesh boundaries to increase the numerical dissipation. Stretching is expected to lower the numerical reflections on upstream and downstream boundaries because the present nonreflecting boundary conditions (NRBC) are based on the Thomson condition (see Hixon[22]) known to be suitable only for plane waves.

Details about grid points and CPU time requirement are given in Sec. V devoted to a turbofan model simulation case studied in the framework of Basic Research Duct Acoustics and Radiation (DUCAT) European Project simulations.

B. Euler Computations

Acoustic propagation is simulated using the three-dimensional structured multiblock platform SABRINA, used here in the Euler mode. Details about the solver may be found in Ref. 15. For engine noise problems, the code is particularly able to solve the full Euler equations applied to the disturbances, aiming at simulating acoustic propagation in complex flows (as for jet noise or shock waves in transonic conditions). As mentioned in the Introduction, for the case of isentropic subsonic flows, these equations should be considered roughly equivalent to usual LEE, as for present applications. SABRINA uses a low dispersive sixth-order scheme in space and a third-order Runge–Kutta scheme for the time integration. Efficient NRBC under development should be soon available in SABRINA. However, the conventional Thomson approach enhanced by a grid stretching is used in the present study to simulate free-space conditions. Nondispersive and nondissipative acoustic propagation is ensured using $\lambda/10$ grid spacing in the axial direction, where λ is the smallest axial wavelength. The time spacing is adjusted so that the Courant–Friedrich–Lewy number is close to 1, to limit the number of time iterations required to obtain a periodical solution. CPU time for three-dimensional applications is roughly equal to 2.5 μs/point/iteration on a NEC SX5.

Generation of basic source terms (monopoles, quadrupoles) in SABRINA is available and currently used.[16] Normalized monopoles have been recently implemented to simulate a spatial Dirac distribution (point-source with unity amplitude) required by the coupling method described in Sec. III. Details are given in the Appendix, Sec. A.

C. Far-Field Predictions Using Kirchhoff

Because interaction noise simulations are practically limited to first BPF tones (generated here by means of harmonic sources in the Euler code), the Kirchhoff time-formulation (see Ref. 17) is written in the frequency domain. It prevents additional interpolation (time integration), and it is much more convenient with respect to data storage and CPU time requirement (being then both negligible). Far-field harmonic pressure is deduced from the following integral:

$$p_\omega(x,t) = \frac{1}{4\pi d}\int_{S_k}\left[M^2\cos\varphi\frac{\partial p}{\partial z} - \frac{\partial p}{\partial n} + \left\{ iK\left(M\cos\varphi + \frac{n_i(x_i-y_i)}{d}\right) + \beta^2\frac{n_i(x_i-y_i)}{d^2}\right\}p\right]e^{i(\omega t - K\sigma)}\,\mathrm{d}S$$

The acoustic pressure field provided by SABRINA along selected grid surfaces has first to be Fourier transformed. Three adjacent surfaces are practically used to compute the pressure gradient. Although the Kirchhoff routine directly uses the CAA grid data (with no interpolation required), the shape of the Euler grid is designed to be roughly hemispherical with almost regular spacing in the vicinity of the Kirchhoff surface location to reduce numerical errors. Euler/Kirchhoff coupling has been checked and validated by comparisons with analytical solutions and BEM simulations (Sec. V).

III. Equivalent Source Model

The propagation model proposed to match RANS and Euler calculation is the solution of the convected Helmholtz equation in an annular duct. The uniform mean flow assumption should be restricted for the upstream region of the fan because the vorticity and the boundary layer are negligible in this area far from the wake

region. However, these assumptions nowadays may be adopted also for the bypass duct exhaust,[8] as long as the CFD/CAA matching problem for rotational flows does not encounter any practical issues. Extension of the modal expansion in shear flows is made possible by using the Pridmore–Brown equation, which can be solved using standard numerical techniques (see Ref. 23), but eigensolutions are not fully reliable because the modes are not orthogonal and the completeness of the eigensystem is not yet guaranteed. For the subsonic rotor conditions, the inlet flow can be described by potential equations and the mean velocity remains roughly constant as long as the duct section varies slowly (flow-rate conservation). Rienstra and Eversman propose a more general multiple-scale solution taking into account a slowly varying duct section,[24] but here we limit to the more conventional uniform-flow/annular-duct assumption to obtain a simple mathematical expression of Green's function, to get back easily to the sources, as proposed by the equivalent source model to be described.

Acoustic pressure is expanded over spinning and radial modes (m, μ) as follows:

$$p(z, r, \theta, t) = \sum_{m,\mu} p^{\pm}_{m\mu} C_{m\mu}\left(\alpha_{m\mu} r^*\right) \exp[i(\omega t - m\theta - k^{\pm} z)] \quad (1)$$

$C_{m\mu}$ are the dimensionless $(r^* = r/R)$ eigenfunctions,[25] and $\pm$ denotes outgoing, $+$, or incoming, $-$, waves. When it is assumed that the fan duct is annular in the matching region, $p_{m\mu}$ can be calculated from the unsteady pressure disturbances provided by CFD in a cross section $(z = z_0)$ upstream of the fan using the following Fourier–Bessel transform:

$$p_{m\mu} = \frac{\omega}{4\pi^2} \int_0^{2\pi/\omega} \int_0^{2\pi} \int_h^1 p\left(z_0, r^*, \theta, t\right) C_{m\mu}\left(\alpha_{m\mu} r^*\right) \times \exp[-i(\omega t - m\theta - k z_0)] r^* \, \mathrm{d}r^* \, \mathrm{d}\theta \, \mathrm{d}t \quad (2)$$

In addition, an efficient wave-splitting technique,[26] consisting of identifying and canceling the incoming waves [k^- in Eq. (1)] is used to suppress the contributions due to the numerical reflections from the CFD mesh boundaries. With use of Green's function, the acoustic pressure profile relative to angular mode of order m can be similarly generated by means of equivalent monopoles:

$$p_m(r) = \sum_{\mu=1}^{\mu_{\max}} \sum_{j=1}^{j_{\max}} q^j A^j_{m\mu}\left(r^j_s\right) C_{m\mu}\left(\alpha_{m\mu} r^*\right) \quad (3)$$

$A_{m\mu}$ represents an elementary solution of LEE for the annular duct/uniform mean flow problem in the presence of a monopole source j at r_s. It is related to the expanded Green's function $G_{m\mu}$ (solution of the convected Helmholtz equation with a Dirac point source). The analytical expression of $G_{m\mu}$ and the way to obtain $A_{m\mu}$ are addressed in Appendix Secs. B and C, respectively.

The amplitude of each monopole q^j, relative to a single mode m, is obtained by using an inverse method consisting in solving the following matrix system:

$$\left[A^j_{m\mu}\left(r^j_s\right)\right]\left[q^j_m\left(r^j_s\right)\right] = [p_{m\mu}] \quad (4)$$

A solution only exists for Eq. (4) under the condition $j_{\max} \geq \mu_{\max}$, where $\mu_{\max}$ is the maximum order of radial modes considered. Note that there is no restriction about evanescent modes (k complex) that can be also included in the model. It is known that such an inverse problem does not have a unique solution (one solution for a given set of source locations). Practically, we set $j_{\max} = \mu_{\max}$, and sources are supposed to be equally distributed in the radial direction. The selected spinning mode order m is generated using a point-source ring ($m\theta$ phase-shifted in the angular direction). This is also described in the Appendix, Sec. A.

IV. Simulations of Acoustic Mode Propagation in an Infinite Annular Duct

The present matching method is checked in the case of an infinite annular duct with a uniform mean flow. (The matching using BEM was proposed and validated in Ref. 18 for a fluid at rest.) The duct geometry is defined by $R = 0.25$ m and $h = 0.67$, and the source frequency is equal to 2500 Hz. A typical grid used is shown in Fig. 2. Because Thomson's NRBC used at duct ends are expected to generate reflected waves, infinite duct conditions are obtained by adjusting the length size (with respect to axial wavelength) and by limiting the number of time iterations.

Table 1 Eigenvalues with associated axial wave numbers

$\alpha_{41} = 4.796$; $\alpha_{42} = 10.76$	Mach = 0	Mach = 0.4
$\lvert k_{41}\rvert$ upstream/downstream, m^{-1}	42/42	72.9/28.8
$\lvert k_{42}\rvert$ upstream/downstream, m^{-1}	16.8/16.8	50.7/6.6

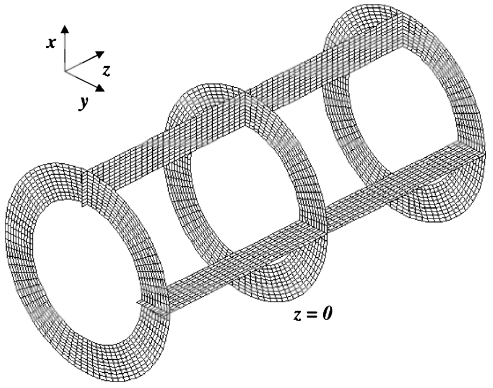

Fig. 2 Annular duct grid used for benchmark.

A harmonic pressure field is expanded over the spinning modes $(m = 4, \mu = 1)$ and $(m = 4, \mu = 2)$, where modes (4,3) and higher are cut-off. When time and angular dependency are omitted (axisymmetrical solution in the frequency domain), the acoustic pressure (3) becomes

$$p(z, r) = \sum_{\mu=1}^{\mu=2} p_{4\mu} C_{4\mu}\left(\alpha_{4\mu} r^*\right) e^{-ik_{4\mu} z}$$

Both the eigenvalues and the upstream/downstream axial wave numbers are summarized in Table 1.

The matrix system (4) to be solved reduces to a two-equation system with two unknowns, q^1 and q^2,

$$q^1 A^1_{41} + q^2 A^2_{41} = p_{41}, \qquad q^1 A^1_{42} + q^2 A^2_{42} = p_{42} \quad (5)$$

Two cases are studied (with pressure-mode amplitude imposed upstream): 1) $p_{41} = 0$ and $p_{42} = 1$, pure second-order radial mode and 2) $p_{41} = 1$ and $p_{42} = 1$, mixed first- and second-order radial modes. Comparisons between the analytical and the numerical solutions are presented in Figs. 3–7.

Figures 3 and 4 show three-dimensional comparisons relative to case 1, without and with flow, respectively. Equivalent source plane (monopoles q^1 and q^2) located at $z = 0$ is indicated. The agreement between analytical and numerical solutions is very good. In particular, the expected convection effect (Fig. 4 compared to Fig. 3) with respect to the axial wavelength and pressure mode amplitude breakdown is perfectly achieved.

The more complex case 2 is analyzed in Fig. 5, showing a similar three-dimensional comparison (with flow). Interference patterns caused by the superposition of the two axial waves are perfectly assessed, as well as convection effects. A comparison in a xz plane, $\theta = 0$ deg, is shown in Fig. 6, to highlight the accuracy of the simulations. Finally, some profile comparisons are shown in Fig. 7 for radial profile ($z = -0.5$ m, Fig. 7a) and axial profile ($r = hR$, Fig. 7b and $r = R$, Fig. 7c). The agreement is excellent between theory and predictions. Reliability of numerical results therefore validates the equivalent source model implemented in SABRINA.

V. Application to the DUCAT Configuration

A. Turbofan Model

The experimental setup of the turbofan model in the DNW–LLF anechoic wind tunnel[20] is shown in Fig. 8. The model consists of

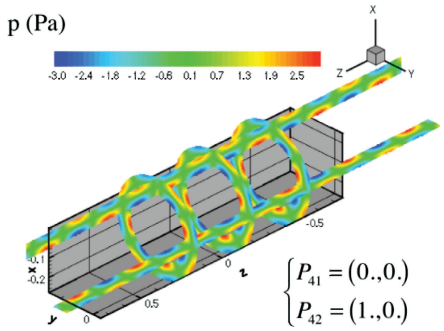

a) Analytical solution

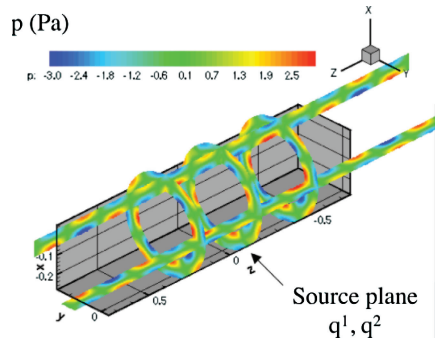

b) Numerical simulation (SABRINA)

Fig. 3 Three-dimensional comparison between analytical and numerical solutions: case 1, Mach = 0.

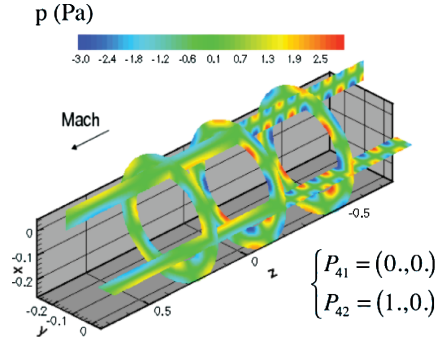

a) Analytical solution

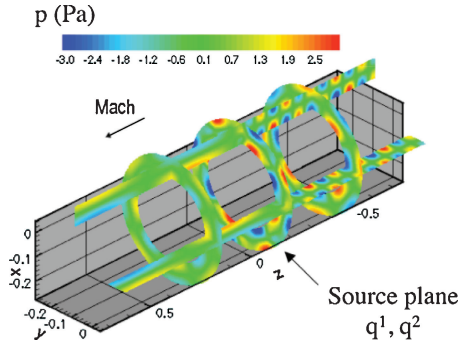

b) Numerical simulation (SABRINA)

Fig. 4 Three-dimensional comparison between analytical and numerical solution: case 1, Mach = 0.4.

a one-stage compressor made of 16 cylindrical rods (rotor) and 18 vanes (stator). Rotor blades, that is, rods, are basically unloaded, and noise generation is essentially due to interaction between the rods wake and the stator vanes. The duct is annular, with $R = 0.2$ m and $h = 0.6$. The flow velocity is uniform and has been adjusted to be almost identical inside and outside the duct (Mach numbers equal to 0.25 and 0.2, respectively). Furthermore, only one mode due to rods–stator interaction is cut on at BPF. All of these parameters make this case well suited for the purpose of code validation.

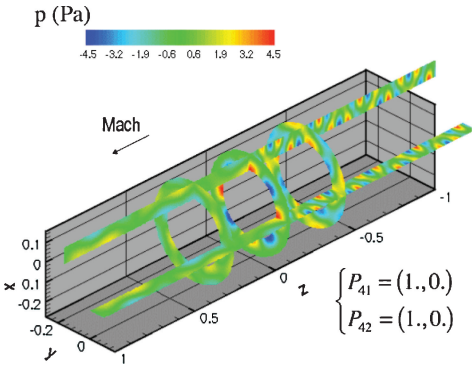

a) Analytical solution

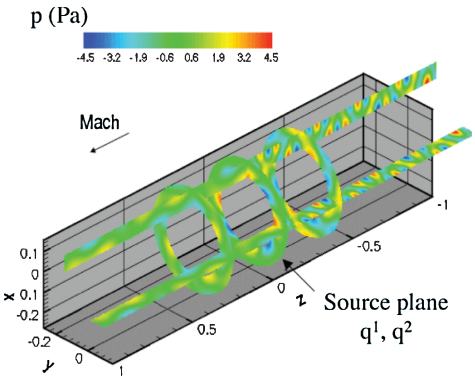

b) Numerical simulation (SABRINA)

Fig. 5 Three-dimensional comparison between analytical and numerical solution: case 2, Mach = 0.4.

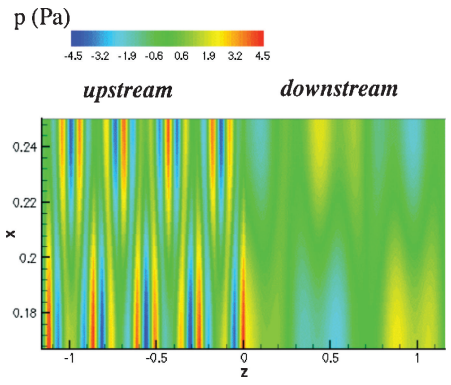

a) Analytical solution

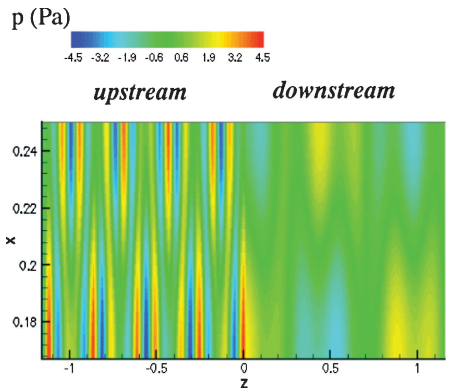

b) Numerical simulation (SABRINA)

Fig. 6 Comparison between analytical and numerical solution, (*xz*) section: case 2, Mach = 0.4.

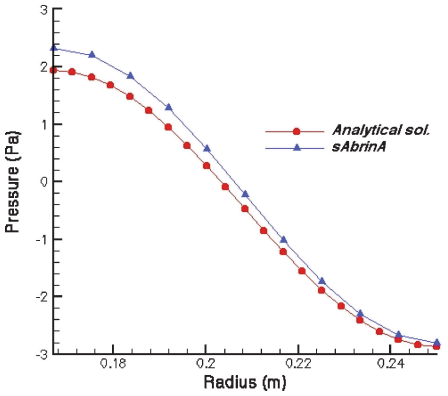

a) Radial profile, $z = -0.5$ m

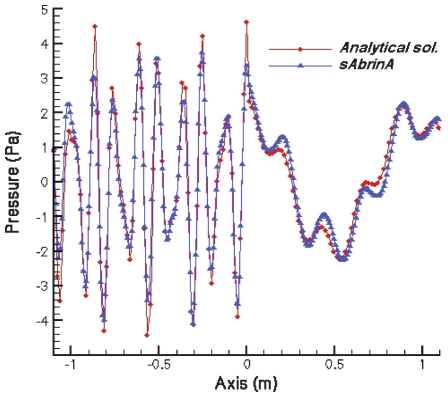

b) Axial profile, $r = hR$

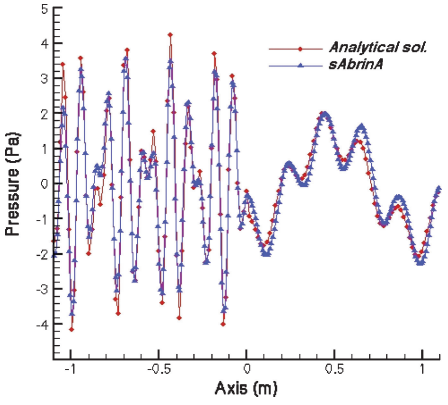

c) Axial profile, $r = R$

Fig. 7 Pressure profile comparisons from analytical and numerical solutions: case 2, Mach = 0.4.

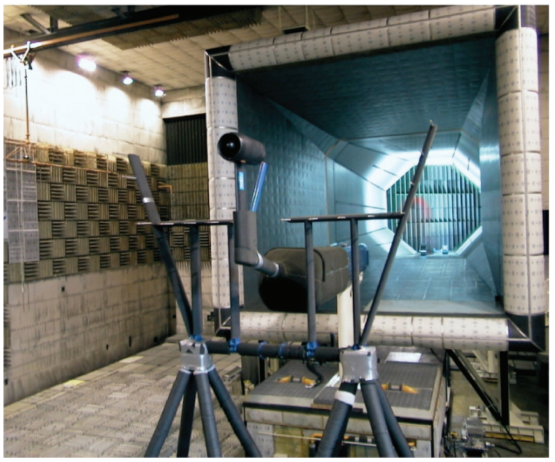

Fig. 8 Experimental setup of DUCAT tests in DNW–LLF.

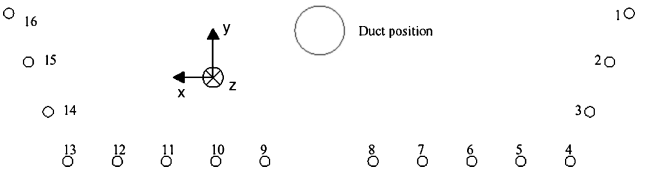

Fig. 9 Microphone position mounted on z-moving rake used for DUCAT tests.

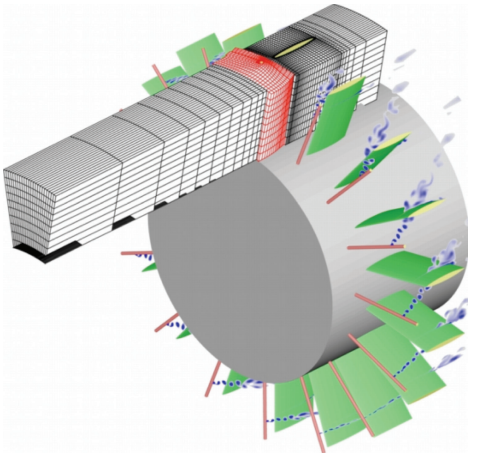

Fig. 10 DUCAT turbofan model with CFD multiblock grids and simulated wakes.

At a rotational speed of 298.5 rad $\cdot$ s^{-1}, BPF is equal to 760 Hz ($KR \approx 3$), and the interaction cut-on mode (m, μ) is $(-2,1)$. The pressure modal amplitude on the outer wall was measured using a 22-microphone ring. Directivity patterns along several planes perpendicular to the duct axis upstream of the rotor were scanned using a 16-microphone rake (seen in Fig. 8) moving along the z axis. Microphone positions with respect to the fan are shown in Fig. 9.

B. Numerical Simulations

Because Reynolds number based on rod diameter (3 mm) is rather low ($Re = 2.4 \times 10^4$) RANS simulations are performed without a turbulence model (laminar flow assumption), which makes convergence quite fast, although it is a crude assumption.

To reduce the computational effort without altering the accuracy of noise sources, a straight annular duct is considered. (Inlet and outlet geometry is not modeled.) The grid is made of 12-structured blocks, the block upstream of the rotor being designed to propagate the outgoing acoustic waves accurately. The CFD grid, the blade and vane surface mesh, and the rotor wake (entropy field snapshot) are presented in Fig. 10. Hence, a total number of 1,260,000 points is used, and about 124 h of CPU time on a NEC-SX5 are required to simulate two full rotor revolutions (corresponding to 230,000 iterations).

SABRINA computations are performed using a monodomain structured grid of $(15 \times 100 \times 156)$ cells along the r, θ, and z directions (Fig. 11). A zero thickness profile is considered for the nacelle to limit the computation domain. For this basic configuration, the in-duct mean flow is nearly uniform so that inlet/exhaust propagation can be simultaneously computed with no restriction. With the assumption that rotor screen effect and scattering through the stator are small (which is probably true because rods are used and because BPF is low), upstream matching only, that is, a single source-plane upstream the rotor, should be sufficient. Hence, both inlet and outlet parts are meshed to take into account (via the Kirchhoff integral) interferences between upstream and downstream radiation that highly modify the directivity shape on BPF.[19] Special attention has been paid to the mesh definition in the source region (where roughly regular cells are used), nearly beyond inlet and outlet cross sections (for accurate coupling with the Kirchhoff integral) and in the vicinity of external boundaries (where the cell size is stretched from 10 to 1 point per wavelength). About 3 h (8000 iterations) of CPU time is required here to get a periodical solution in the entire domain. Note

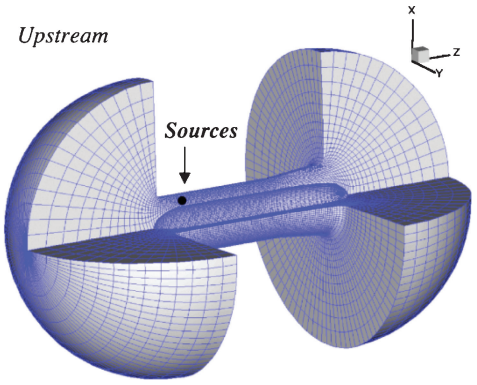

a) Three-dimensional view with equivalent sources location

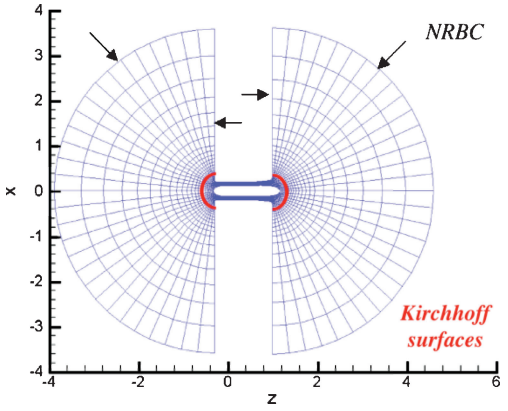

b) Two-dimensional view with Kirchhoff surface location

Fig. 11 CAA grid used for SABRINA and Kirchhoff computations.

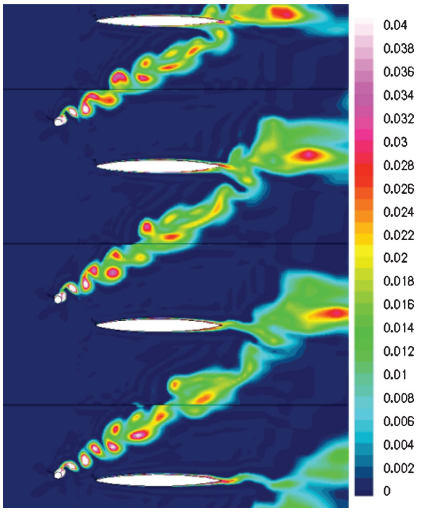

Fig. 12 Entropy snapshot resulting from phase-lagged approach.

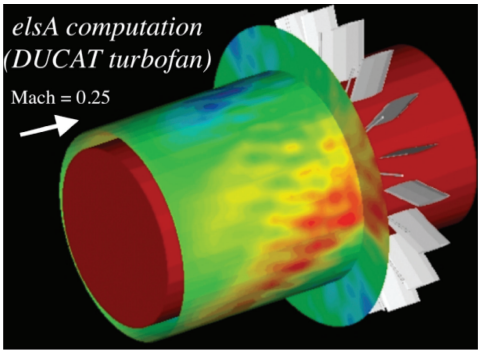

a) Three-dimensional view

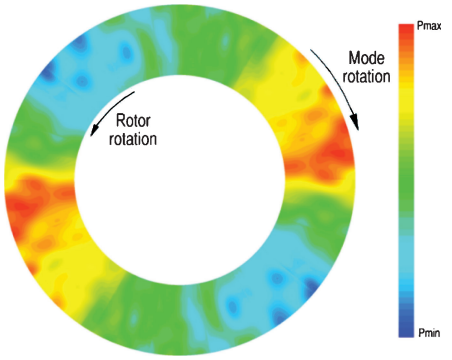

b) Section view

Fig. 13 Instantaneous pressure field simulated by RANS showing interaction cut-on mode (−2,1).

that in axisymmetric geometry, periodicity conditions have been recently implemented by Redonnet, so that an angular sector of $2\pi/m$ is sufficient (instead of a full-revolution grid).

C. Results and Validations

Von Kármán vortex streets that are present downstream of the rods (Fig. 10) could suggest that the flow does not fully match the phase-lagged assumption. This is probably the most critical point of this type of RANS simulations if rods are used instead of real blade airfoils. Nevertheless, periodicity is almost achieved, as is shown by the entropy snapshot plotted in Fig. 12, despite a slight discontinuity on each interface. The expected interaction mode (−2,1) is generated and propagated, as revealed in the instantaneous pressure field shown in Fig. 13.

CFD postprocessed pressure, in the cross section $z_0 = -0.09$ m is compared in Fig. 14 to the Fourier–Bessel harmonic of order (−2,1) [$C_{21}(\alpha_{21}r)$ in Eq. (2)]. Accord is nearly perfect, which proves the reliability of the simulations. The computed angular mode spectrum on the outer wall is compared to the experiment in Fig. 15.

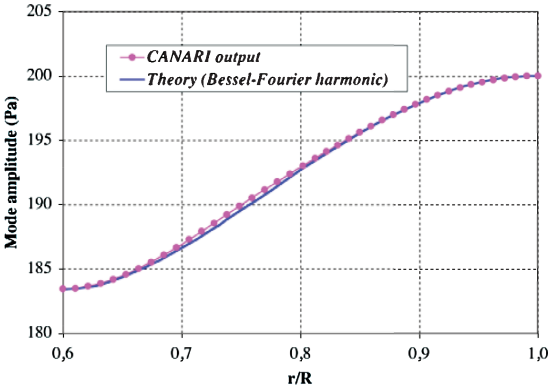

Fig. 14 Comparison between in-duct pressure profiles on BPF.

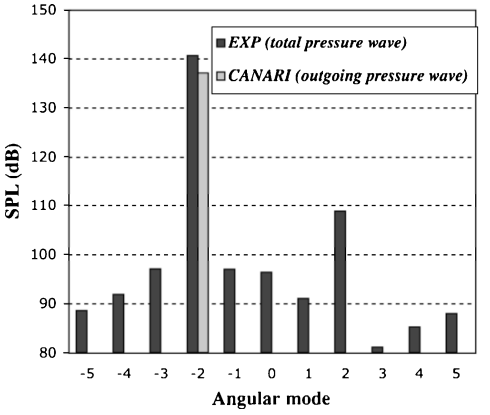

Fig. 15 Angular mode spectrum (BPF) on outer wall.

The expected interaction mode $m = -2$ is found to be largely dominant over other cut-on modes (at least 30 dB higher in tests and more than 60 dB in the simulations). Note that contrary to the in-duct measurements, providing a total acoustic pressure field including incoming reflected fields from inlet and outlet (due to impedance discontinuity), the CFD here simulates an outgoing wave, which can partly explain the small gap level at $m = -2$.

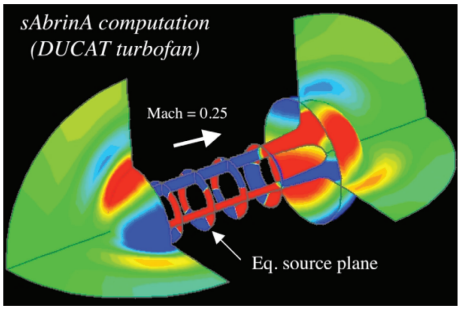

Fig. 16 Simulation of interaction mode propagation/radiation with SABRINA.

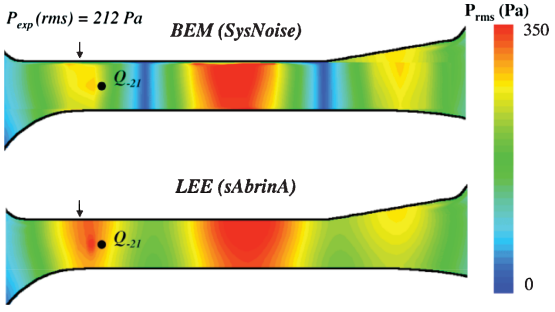

Fig. 17 Numerical simulations of in-duct propagation (no flow) using BEM (top) and LEE (bottom).

The simulation of in-duct propagation and radiation by inlet and exhaust using SABRINA is presented in Fig. 16. Because only the first radial mode is cut on, a single point-source ring, whose amplitude is deduced from Eq. (4), is needed. At least 20 periods (8000 time iterations) are necessary to achieve periodicity, requiring 3 h of CPU time on a NEC SX5. Simulations are also performed without flow to be compared to the BEM previous results.[18] In-duct propagation simulated using BEM and LEE is shown in Fig. 17. Modal pressure measured on the outer wall (Fig. 15) is also indicated. Shape and amplitude of predicted rms pressure fields, clearly showing standing waves, are in good agreement.

The acoustic field radiated by inlet and outlet is presented in Fig. 18, which shows a comparison of direct Euler simulation (Fig. 18a) with SABRINA/Kirchhoff solution (Fig. 18b). Upstream and downstream Kirchhoff surfaces are also indicated. Agreement between near-field predictions is good, but the coupling with Kirchhoff seems to give a more accurate directivity pattern farther away than the direct simulation. (It tends to dissipate consequently to the stretching of the grid.) The total pressure field radiated upstream (including both inlet and outlet contributions) obtained using LEE/Kirchhoff is then presented in Fig. 19b. It is compared to the BEM solution shown in Fig. 19a. Predicted directivity reveals distinct lobes with clearance patterns, similarly assessed by each computation, with only some minor discrepancies.

Finally, sound pressure level (SPL) directivity patterns at microphone locations are compared to experiment in Fig. 20, for three axial positions of the microphone rake. Directivity shapes are in fairly good agreement. In particular, the cancellations due to interferences between forward and rearward radiations are well assessed by the simulations (Figs. 20b and 20c). SPLs are in a quite good agreement, too, if predicted level fits the measurements on the duct outer wall (as is done here). Predictions without adjusting inputs are also plotted (top curve) in Fig. 20a, showing an overestimation of about 5 dB over the experiment. This discrepancy can be attributed to some uncertainties of the intensity of the interaction mode that seems to be overpredicted, probably because no turbulence model was used to simulate the rod wakes.

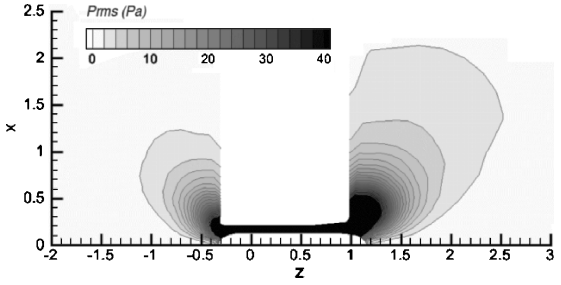

a) Equivalent sources plus SABRINA **b) Equivalent sources plus SABRINA/Kirchhoff**

Fig. 18 Radiated field simulated using direct Euler and Euler/Kirchhoff computations.

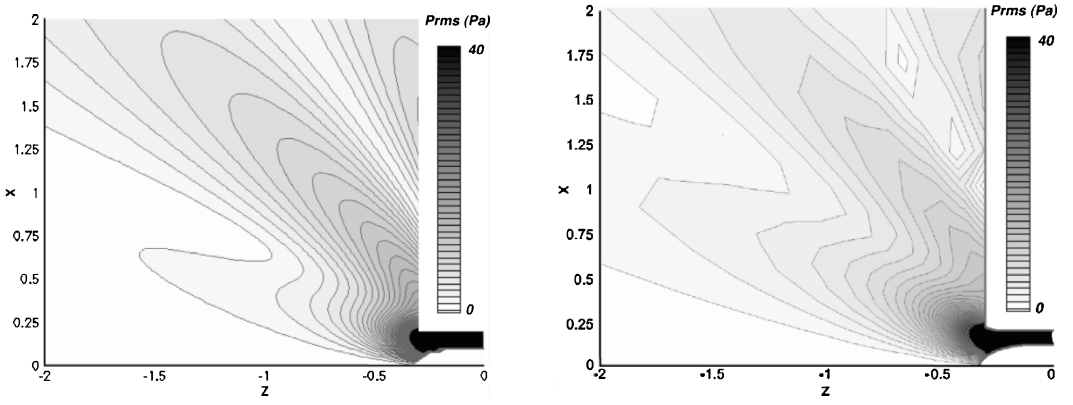

a) BEM (SysNoise) **b) SABRINA/Kirchhoff (inlet plus outlet contributions)**

Fig. 19 Comparison between BEM and Euler/Kirchhoff simulations of aft-radiated field (no flow).

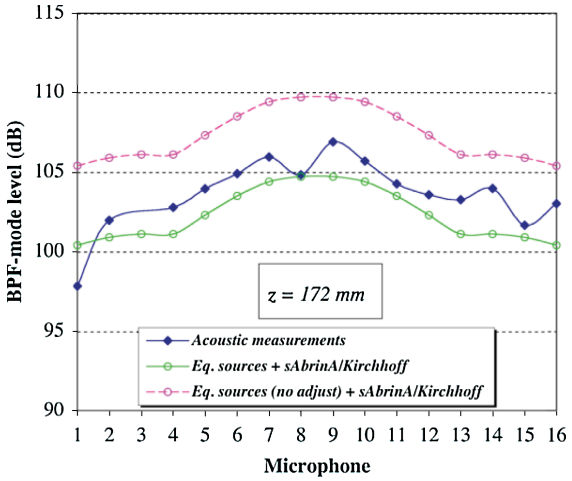

a) $z = -172$ mm

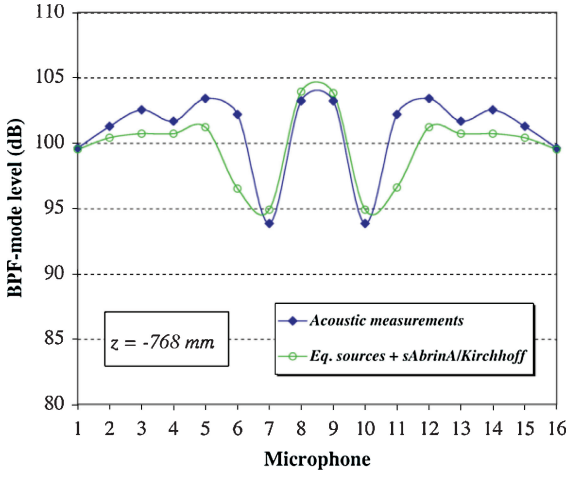

b) $z = 768$ mm

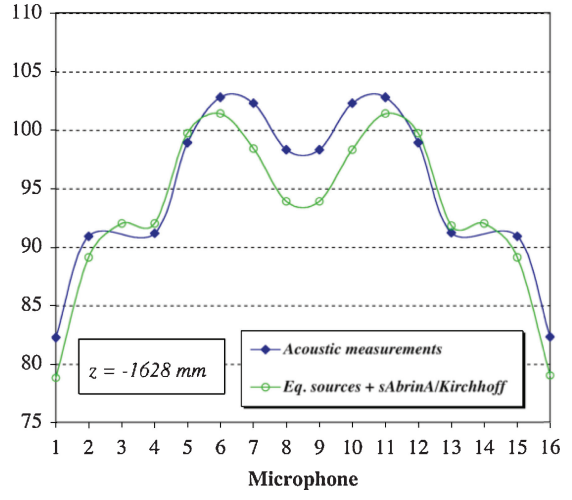

c) $z = 1628$ mm

Fig. 20 Predicted and measured directivity patterns at three axial positions of 16-microphone rake.

VI. Conclusions

A source-to-far-field computation procedure has been presented and successfully applied to a turbofan model. A modal expansion approach is used to couple a three-dimensional RANS code, designed for noise source generation, to a Euler/Kirchhoff code, designed for acoustic propagation and radiation. Equivalent monopoles aimed at regenerating the acoustic field deduced from modal expansion are entered as source terms in the Euler code. First results are very promising because predicted SPL directivities are within 1 dB of the experiment if CFD postprocessed outputs are adjusted to fit the in-duct measurements. As regards overestimated levels using the CFD inputs, the interaction mode amplitude provided by the RANS solution seems to be overpredicted, probably because no turbulence model was used for rotor wake simulation. The capability of present three-dimensional simulations to generate, propagate, and radiate interaction noise, including flow and interference effects, has been demonstrated, and the methodology proposed appears to be valid.

The next step will extend the computations to industrial configurations in nonuniform flow and in the presence of several cut-on modes (predictions on two BPF and three BPF). This work is underway and should be applied to ultra-high bypass ratio and contrarotating fans, in the framework of future European projects.

Appendix: Equivalent Source Terms Implementation

A. Harmonic (Spinning) Point-Source Implementation in SABRINA

The Euler disturbance equations with source terms written in a linearized nonconservative form are

$$\frac{\mathrm{d}\rho}{\mathrm{d}t} + \rho_0 \nabla \times u = s_\rho, \qquad \rho_0 \frac{\mathrm{d}u}{\mathrm{d}t} + \nabla p = s_u$$

$$\frac{\mathrm{d}p}{\mathrm{d}t} + \gamma p_0 \nabla \times u = s_p \tag{A1}$$

The uniform mean flow derivatives are

$$\frac{\mathrm{d}}{\mathrm{d}t} = \frac{\partial}{\partial t} + U_0 \times \nabla \tag{A2}$$

The isentropic acoustic mode is given as

$$s_p = s_\rho c_0^2, \qquad s_u = 0, \qquad c_0^2 = \gamma p_0/\rho_0 \tag{A3}$$

The nonhomogeneous convected wave equation, deduced from Eqs. (A1–A3), is

$$p - \frac{1}{c_0^2}\frac{\mathrm{d}^2 p}{\mathrm{d}t^2} = -\frac{\mathrm{d}s_\rho}{\mathrm{d}t}$$

The harmonic point source is

$$s_\rho(x, y, z, t) = (1/b^3)\exp[-\pi(\hat{r}^2/b^2)]\sin(\omega t)$$

$$b = (\Delta x^2 + \Delta y^2 + \Delta z^2)^{\frac{1}{2}}$$

$$\hat{r} = \left[(x - x_s)^2 + (y - y_s)^2 + (z - z_s)^2\right]^{\frac{1}{2}}$$

$$s_\rho(t) = \delta(r - r_s)\sin(\omega t), \qquad b \to 0$$

where $\Delta =$ grid spacing.

The spinning mode of order m using point-source ring is

$$s_\rho(r, \theta, z, t) = \left(1/2\pi r_s b^2\right)\exp[-\pi(\hat{r}^2/b^2)]\sin(\omega t - m\theta)$$

$$\hat{r} = \left[(r - r_s)^2 + (z - z_s)^2\right]^{\frac{1}{2}}, \qquad \theta = \tan^{-1}(y/x)$$

B. Green's Function Solution of Convected Helmholtz Equation in an Infinite Annular Duct

The nondimensioned convected Helmholtz equation with a Dirac source term is

$$\Delta p^* - \left(i\omega^* + M\frac{\partial}{\partial z}\right)^2 p^* = \delta\left(r^* - r_s^*\right)$$

$$p^* = \frac{p}{\rho_0 c_0^2}, \qquad r^* = \frac{r}{R}, \qquad \omega^* = K^* = \frac{\omega R}{c_0}, \qquad \delta(r^*) = R\delta(r)$$

The expanded Green function for an infinite annular duct (eigenfunctions from Ref. 25) is

$$G^*_{m\mu}\left(r^*\middle|r^*_s\right) = i\left[C_{m\mu}\left(\alpha_{m\mu}r^*_s\right)\middle/4\pi\,\Delta_{m\mu}\right]$$
$$\times C_{m\mu}(\alpha_{m\mu}r^*)\exp[-i(\omega\tau + m\theta + kz)]$$
$$= \Gamma_{m\mu}\left(r^*_s\right)C_{m\mu}\left(\alpha_{m\mu}r^*\right)\exp[-i(\omega\tau + m\theta + kz)]$$

$$G_{m\mu} = G^*_{m\mu}\big/R$$

where dimensions are per meter and

$$\Delta_{m\mu} = \sqrt{\left(\omega^{*2} - \beta^2\alpha^2_{m\mu}\right)}, \qquad k^* = \frac{-M\omega^* \pm \Delta_{m\mu}}{\beta^2}$$

$$C_{m\mu}\left(\alpha_{m\mu}r^*\right) = N_{m\mu}\cos(\tau_{m\mu})J_m\left(\alpha_{m\mu}r^*\right)$$
$$- N_{m\mu}\sin(\tau_{m\mu})Y_m\left(\alpha_{m\mu}r^*\right)$$

$$N_{m\mu} = \frac{\sqrt{2}}{2}\pi\alpha_{m\mu}\left[\frac{\left(1 - m^2\big/\alpha^2_{m\mu}\right)}{J'^2_m(\alpha_{m\mu}) + Y'^2_m(\alpha_{m\mu})}\right.$$
$$\left. - \frac{\left(1 - m^2\big/\alpha^2_{m\mu}h^2\right)}{J'^2_m(\alpha_{m\mu}h) + Y'^2_m(\alpha_{m\mu}h)}\right]^{-\frac{1}{2}}$$

$$\tau_{m\mu} = \tan^{-1}\left[\frac{J'_m(\alpha_{m\mu})}{Y'_m(\alpha_{m\mu})}\right]$$

The plane wave solution [mode (0,1)] is

$$G_{01} = (i/2\pi)[1/KR^2(1 - h^2)]e^{-i(\omega\tau + kz)}$$

C. LEE Solution in Annular Duct with Uniform Mean Flow and a Monopole Source Term

The convected wave equation with a monopole-source term (defined from LEE) is

$$p - \frac{1}{c_0^2}\frac{\mathrm{d}^2p}{\mathrm{d}t^2} = -Q(t)$$

$$s(r|r_s, t) = \delta(r - r_s)\sin(\omega t) = \delta(r - r_s)Re\{-ie^{i\omega t}\}$$

$$Q(t) = \frac{\mathrm{d}s}{\mathrm{d}t}$$

The Fourier transformed solution is

$$p_\omega = TF\{Q \times G\} = TF\left\{\frac{\mathrm{d}s}{\mathrm{d}t} \times G\right\}$$
$$= TF\{-s\}TF\left\{\frac{\mathrm{d}G}{\mathrm{d}\tau}\right\} = i\frac{\mathrm{d}G_\omega}{\mathrm{d}\tau}$$

$$\frac{\mathrm{d}}{\mathrm{d}\tau} = \frac{\partial}{\partial\tau} + c_0M\frac{\partial}{\partial z_s} = \frac{\partial}{\partial\tau} - c_0M\frac{\partial}{\partial z}$$

The determination of modal factor amplitude $A_{m\mu}$ used by the inverse method (equivalent source model) is

$$p(z, r, \theta, t) = Re\{p_\omega(z, r, \theta)\exp(i\omega t)\}$$
$$= Re\left\{\sum_{m\mu}A_{m\mu}C_{m\mu}\left(\alpha_{m\mu}r^*\right)\exp[i(\omega t - m\theta - kz)]\right\}$$

$$A_{m\mu}(r_s) = i\frac{\mathrm{d}G_{m\mu}}{\mathrm{d}\tau}C^{-1}_{m\mu}\left(\alpha_{m\mu}r^*\right)\exp[i(\omega\tau + kz + m\theta)]$$
$$= i(-i\omega + ic_0Mk)\Gamma_{m\mu}(r_s)$$

$$A_{m\mu}(r_s) = (\omega - c_0Mk)\Gamma_{m\mu}(r_s)$$

Acknowledgment

The authors thank the European Commission for its financial support for both the DUCAT and TurboNoiseCFD projects.

References

[1]Couaillier, V., "Recent Developments Performed at ONERA for the Simulation of 3D Inviscid and Viscous Flows," 11th International Symposium on Air Breathing Engines, ISABE, Sept. 1993.

[2]Billonnet, G., Fourmaux, A., and Toussaint, C., "Evaluation of Two Competitive Approaches for Simulating the Time-Periodic Flow in an Axial Turbine Stage," 4th European Conf. on Turbomachinery, March 2001.

[3]Cambier, L., and Gazaix, M., "elsA: An Efficient Object-Oriented Solution to CFD Complexity," AIAA Paper 2002-108, Jan. 2002.

[4]Rumsey, C. L., Biedron, R. T., Farassat, F., and Spence, P. L., "Ducted-Fan Engine Acoustic Predictions Using a Navier–Stokes Code," *Journal of Sound and Vibration*, Vol. 213, No. 4, 1998, pp. 643–664.

[5]Ahuja, V., Ozyoruk, Y., and Long, L. N., "Computational Simulations of Fore and Aft Radiation from Ducted Fans," AIAA Paper 2000-1943, June 2000.

[6]Biedron, R. T., Rumsey, C., Podboy, G. G., and Dunn, M. H., "Predicting the Rotor–Stator Interaction Acoustics of a Ducted Fan Engine," AIAA Paper 2001-0664, Jan. 2001.

[7]Ali, A. A., Atassi, O. V., and Atassi, H. M., "Derivation and Implementation of Inflow/Outflow Conditions for Aeroacoustic Problems with Swirling Flows," AIAA Paper 2001-2173, May 2001.

[8]Zhang, X., Chen, X. X., Morfey, C. L., and Tester, B. J., "Computation of Fan Noise Radiation Through a Realistic Engine Exhaust Geometry with Flow," AIAA Paper 2003-3267, May 2003.

[9]Nark, D. M., Farassat, F., Pope, D. S., and Vasta, V., "The Development of the Ducted Fan Noise Propagation and Radiation Code CDUCT-LARC," AIAA Paper 2003-3242, May 2003.

[10]Bréard, C., "Acoustic Propagation and Radiation Modeling of Lined Duct with Linear and Non-Linear Frequency-Domain Solver," AIAA Paper 2003-3265, May 2003.

[11]Li, X. D., Schoenwald, N., Yan, J., and Thiele, F., "A Numerical Study on the Acoustic Radiation from a Scarfed Intake," AIAA Paper 2003-3245, May 2003.

[12]Zheng, S., Zhuang, M., and Thiele, F., "Noise Prediction and Optimization System for Turbofan Engine Inlet Duct Design," AIAA Paper 2004-3031, May 2004.

[13]Caro, S., Ploumhans, P., and Gallez, X., "Implementation of Lighthill's Acoustic Analogy in a Finite/Infinite Elements Framework," AIAA Paper 2004-2891, May 2004.

[14]Terracol, M., Labourasse, E., Manoha, E., and Sagaut, P., "Numerical Simulation of the 3D Unsteady Flow in a Slat Cove for Noise Prediction," AIAA Paper 2003-3110, May 2003.

[15]Manoha, E., Redonnet, S., Guenanff, R., and Terracol, M., "Acoustic Scattering From Complex Geometries," AIAA Paper 2004-2398, May 2004.

[16]Redonnet, S., Manoha, E., and Kenning, O., "Numerical Simulation of the Downstream Fan Noise and Jet Noise of a Coaxial Jet with a Shielding Surface," AIAA Paper 2004-2991, May 2004.

[17]Polacsek, C., Zibi, J., Rouzaud, O., and Kuntz, M., "Helicopter Rotor Noise Predictions Using ONERA and DLR Euler/Kirchhoff Methods," *AHS Journal*, Vol. 44, No. 2, 1999, pp. 121–131.

[18]Polacsek, C., and Burguburu, S., "Fan Interaction Noise Predictions Using RANS-BEM Coupling," *International Journal of Aeroacoustics*, Vol. 4, No. 1–2, 2005, pp. 153–167.

[19]Polacsek, C., and Burguburu, S., "Computation of Fan Tone Noise Generation and Radiation from Engine Inlets," 11th International Congress on Sound and Vibration Conf., July 2004.

[20]Rademaker, E. R., "Publishable Synthesis Report DUCAT," Rept. DUCAT-NL-01-T5 9, NLR-TR-2001-170, 2001.

[21]Fourmaux, A., "Assessment of a Low Storage Technique for Multistage Turbomachinery Navier–Stokes Computation," American Society of Mechanical Engineers, Nov. 1994.

[22]Hixon, R., "3-D Characteristic-Based Boundary Conditions for CAA," AIAA Paper 2000-2004, June 2000.

[23]Kousen, K. A., "Eigenmodes of Ducted Flows with Radially-Dependent Axial and Swirl Velocity Components," NASA CR 1999-208881, March 1999.

[24]Rienstra, S. W., and Eversman, W., "A Numerical Comparison Between the Multiple-Scales and Finite-Element Solution for Sound Propagation in Lined Flow Ducts," *Journal of Fluid Mechanics*, Vol. 437, 2001, pp. 367–384.

[25]Rienstra, S. W., "Acoustic Radiation from a Semi-Infinite Annular Duct in Uniform Subsonic Mean Flow," *Journal of Sound and Vibration*, Vol. 94, No. 2, 1984.

[26]Wilson, A. G., "A Method for Deriving Tone Noise Information from CFD Calculations on the Aeroengine Fan Stage," Symposium on Developments in Computational Aero- and Hydro-Acoustics, Oct. 2001.

B. Balachandran
Associate Editor